



Conception and Manufacturing of a Planar Inductance on NiFe Substrate

Fatima Zohra Medjaoui¹ · Azzedine Hamid^{2,3} · Yacine Guettaf³ · Pierre Spiteri⁴ · Vincent Bley⁵

Received: 11 September 2018 / Revised: 10 February 2019 / Accepted: 25 February 2019 / Published online: 7 March 2019
© The Korean Institute of Electrical and Electronic Material Engineers 2019

Abstract

The present paper presents the study, realization and characterization of a micro-coil sandwiched using a relatively thick layer of magnetic material. The integration of this micro-coil with as a starting point a set of specifications, requires the following steps: Identification and validation of geometric parameters for the calculation of electrical parameters. Losses dissipated as heat in these electronic systems are becoming a major concern for designers. This prompted to take into account the thermal design. The results obtained have allowed to realize a micro-coil micro square planar coil sandwiched shaped between two magnetic materials. Several carried measures focused on the inductance and resistance which are related to the frequency f , the module and phase of the impedance, and the gap g . The operation of these data is used to trace the evolution of the inductance value L_s , the quality factor Q and the resistor R_s as a function of frequency.

Keywords Integration · Kapton · NiFe · Planar coil · Micro converter · Dimensioning

1 Introduction

Power electronics is currently evolving towards integration, a consequence of the constraints related to the need for miniaturization but also to reduce manufacturing costs. In

many cases, hybrid systems offer opportunities for volume reduction and the passive components, inductance, transformer and capacitor, represent a brake on this miniaturization. Inductive components such as coils or transformers are key elements of power electronics. These are well known and mastered components with regard to their discrete form, but their integration is still at the study stage and is still far from industrialization. The development of micro-technologies now offers new perspectives for the manufacture of micro-coils adapted to this type of application [1–4]. The main objectives of this work are to study, to show the feasibility of planar spiral inductances “sandwich” between two layers of magnetic materials to limit the problems of EMC (Electromagnetic Compatibility) and to increase the value of the inductance, to highlight the interest of these devices, their advantages and technological difficulties, to check their main characteristics by comparing measurement and simulation. Regarding the topology of our inductance, we retained the square shape because it produces the highest value of inductance. This work is completed by a study of the thermal and electromagnetic behavior of our micro-coil. The work presented in this paper was carried out in the LAPLACE laboratory in Toulouse [5].

✉ Fatima Zohra Medjaoui
fzmedjaoui@yahoo.com

Azzedine Hamid
hamidazdean@yahoo.fr

Yacine Guettaf
y_guettaf@yahoo.fr

Pierre Spiteri
Pierre.Spiteri@enseeiht.fr

Vincent Bley
vincent.bley@laplace.univ-tlse.fr

¹ Department of Electrical Engineering, University of Sciences and Technology of Oran (USTO-MB), Oran, Algeria

² University of Sciences and Technology of Oran, Mohamed BOUDIAF, Oran, Algeria

³ El Bayadh's University Center Nour Bachir, El Bayadh, Algeria

⁴ INP-ENSEEIHT, IRIT, Toulouse, France

⁵ University of Paul Sabatier, LAPLACE Laboratory, Toulouse, France

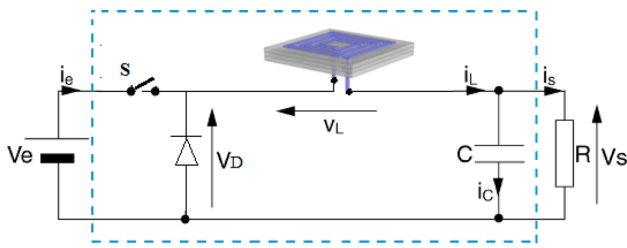


Fig. 1 Schematic diagram of a buck converter

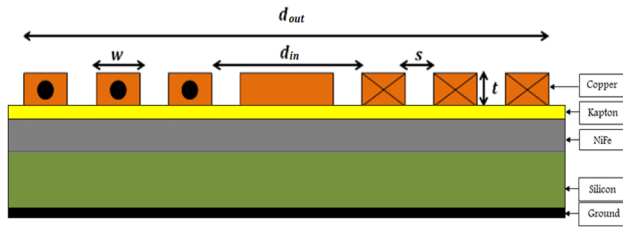


Fig. 2 Sectional view of the inductance on several layers of materials

2 Presentation of Converter

The study is oriented towards a buck converter, which is a DC/DC step-down voltage converter, see Fig. 1. The choice of the structure of the micro-converter was made quite simply, since it is not a question here of trying to find an innovative structure and to study the advantages and disadvantages, but to use a structure of basis so that it can be integrated without much difficulty. Our aim is to design and dimension a planar spiral inductance in order to insert it into the micro-converter. Sizing is done to avoid or eliminate parasitic effects. The thermal and electromagnetic effects are also treated to ensure the good operation of the coil after its insertion into the micro-converter.

2.1 Condition Specifications

The design of a planar coil is an empirical approach and requires several successive and iterative steps, so it is difficult to predict its performance before manufacturing. The aim is to provide a general method for designing a

planar coil. It is possible to calculate the geometrical and electrical quantities of the planar coil as well as the volume of the magnetic core and the surface occupied by the spiral. The initial specification, representing the specific needs of the designer and are established to meet a typical application. It includes: Input voltage: $V_{in} = 5$ V, Output voltage: $V_{out} = 2.5$ V, Output power: $P_{out} = 1$ W, Duty cycle: $\alpha = 0.5$, Operation frequency: $f = 500$ kHz. The choice of the frequency is essential because it conditions the whole of the study, that it is with respect to the active parts of the micro-converter, as compared to the passive elements whose study is made in a second time.

3 Micro-coil Dimensioning

3.1 Micro-coil Geometric Parameter Calculations

The micro coil spiral is geometrically described by several parameters: the width w , the thickness of the conductor t , the inter-spacing of winding s , the number of turns n , the inside diameter d_{in} , and the outside diameter d_{out} and the total conductor length l_t , see Fig. 2 [1, 6]. The d_{in} and d_{out} should be chosen to optimize the relationship between the inductor and the area occupied on the circuit. It is composed of a conductive spiral of copper laid on three stacked layers; a layer of Kapton insulation, a ferromagnetic layer and a silicon semiconductor layer, all put on a ground plane. Characteristics of inductance, substrate and insulation are presented in Table 1.

From a specifications and based on the method of Wheeler modified we will dimension the square planar spiral inductor, with the aim of a minimum losses [1, 2]. The equations below allow to calculate the different geometric parameters mentioned in Sect. 3.1.

$$L_s = k_1 \mu \frac{n^2 d_{avg}}{1 + k_2 \rho} \tag{1}$$

$$n = \sqrt{\frac{2L_s [(1 + c) + k_2(1 - c)]}{\mu_0 k_1 d_{out} (1 + c)^2}} \tag{2}$$

Table 1 Characteristics of inductance, substrate and insulation

Materials	Copper Cu	Kapton K	Ferrite $NiFe$	Silicon Si
Permeability	$\mu_{Cu} = 1$	$\mu_K = 1$	$\mu_{NiFe} = 800$	$\mu_{Si} = 1$
Resistivity (Ω m)	$\rho_{Cu} = 1.75 \times 10^{-8}$	$\rho_K = 15 \times 10^{-2}$	$\rho_{NiFe} = 20 \times 10^{-8}$	$\rho_{Si} = 18.5$
Permittivity	$\epsilon_u = 1$	$\epsilon_K = 3.9$	$\epsilon_{NiFe} = 11.8$	$\epsilon_{Si} = 11.8$
Thickness (μ m)	$t = 50$	$t_K = 7.2$	$t_{NiFe} = 1.93$	$t_{Si} = 50$
Section (mm^2)	$S_{Cu} = (18.14 \times 50) \times 10^{-6}$	$S = 1.7 \times 1.7$	$S = 1.7 \times 1.7$	$S = 1.7 \times 1.7$

$$c = \frac{d_{in}}{d_{out}}, \quad d_{out} = d_{in} + 2n(sw) \tag{3}$$

$$\rho = \frac{d_{out} - d_{in}}{d_{out} + d_{in}} \tag{4}$$

$$l_t = [d_{out} - (n - 1)s - nw] - s \tag{5}$$

$$d_{avg} = \frac{d_{out} + d_{in}}{2} \tag{6}$$

with $k_1 = 2.34$ and $k_2 = 2.75$.

3.2 Micro-coil Electrical Parameter Calculations

Figure 3a, b shows the electrical model.

This model includes the series inductance L_s , the series resistor R_s , the coupling capacitance between the turns C_s , the capacitance associated with the insulation layer (Kapton) t_k with the substrate C_k , the capacity C_{Si} and the resistance R_{Si} of the silicon, Resistance of ferrite R_{NiFe} , show the equivalent scheme in π of a spiral micro coil [1, 2, 4, 6].

$$R_s = \frac{\rho_{Cu} l_t}{S_{Cu}} = \frac{\rho_{Cu} l_t}{wt} \tag{7}$$

$$C_{k1} = C_{k2} = \frac{1}{2} l_t w \frac{\epsilon_0 \epsilon_k}{t_k} \tag{8}$$

$$C_{Si1} = C_{Si2} = w l_t \frac{\epsilon_0 \epsilon_{Si}}{t_{Si}} \tag{9}$$

$$R_{NiFe1} = R_{NiFe2} = \rho_{NiFe} \frac{l_{NiFe}}{S} \tag{10}$$

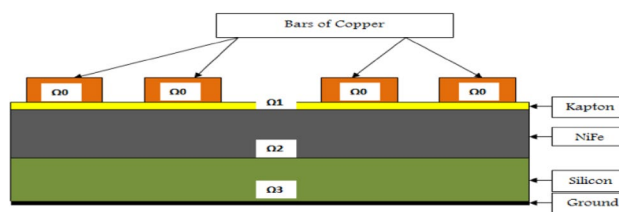
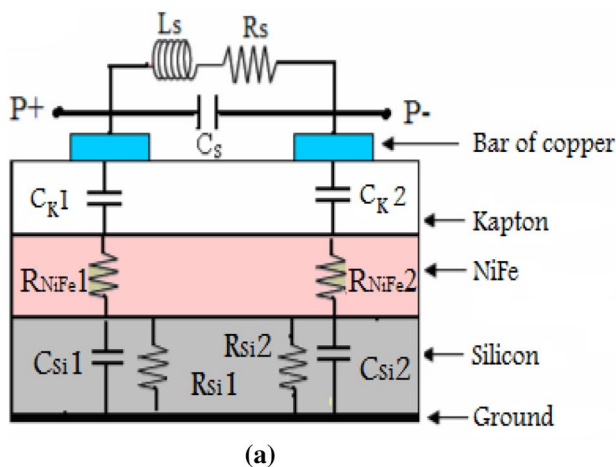


Fig. 4 Two-dimensional model of our component

where t_{NiFe} is the thickness of the magnetic core, which also acts as the substrate and t_k represents the thickness of the Kapton, ρ_{Cu} and ρ are respectively the resistivity of copper and of ferrite and finally ϵ_0 and ϵ_k are the permittivity of vacuum and the Kapton.

3.3 Micro-coil Temperature Calculation

3.3.1 Mathematical Model

In the sequel we consider a two-dimensional layered model described by the heat equation in which the bars of copper, the Kapton, the $NiFe$ and the silicon substrate are considered as continuous and solid surface, see Fig. 4.

The following assumptions are considered [3, 4].

1. Assembled blocks must be rectangular, but may be in the form of a multilayer assembly level.
2. The lateral edges of these blocks must be adiabatic. On the limit of the first block, the temperature is set at room temperature Text.
3. The power dissipation per unit area is placed on the upper face of each block.

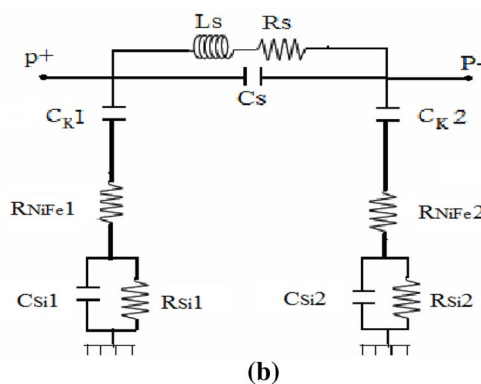


Fig. 3 Equivalent scheme in π of a spiral micro coil [6]

- 4. The thermal conductivity of the different layers constituting each block must be independent of the temperature.

Between each subdomain (layer of each material constituting the component) $\Omega_i, i=0 \dots 3$, a conventional continuity condition at the interfaces corresponding to a heat exchange is considered. Specifically, only the following boundary conditions are taken into account. On the vertical side faces of $\Omega_i, i=0 \dots 3$ the normal flow is taken null:

$$\frac{dT}{dn} = 0 \tag{11}$$

T is the temperature to calculate.

$$-\lambda_i \frac{dT_i}{dy} = \phi_i \tag{12}$$

The continuity conditions at the interfaces, for example between Ω_0 and Ω_1 are given by:

$$\lambda_i \frac{dT_i}{dy} = \lambda_{i+1} \frac{dT_{i+1}}{dy} \tag{13}$$

where λ_i and λ_{i+1} represent the thermal conductivity in Ω_i and Ω_{i+1} , the initial temperature is given by (Where T_a ambient temperature):

$$T(x, y) = T_a. \tag{14}$$

3.3.2 Numerical Solution

For the numerical solution of the heat equation, a spatial discretization by the classical finite difference method is applied. For $i=0 \dots 3$ the vector T_i^n being computed at the previous time step, the vector T_i^{n+1} is obtained by solving the following linear system [4, 7]:

$$(1 + \alpha B_i) \cdot T_i^{n+1} = dt \cdot F_i^{n+1} + T_i^n \tag{15}$$

where B_i is the spatial discretization matrix on $\Omega_i, i=0 \dots 3$, i is the identity matrix and n represents the index of time, $t_n = n dt$, dt being the time step. Let Δx and Δy the spatial discretization steps along the axis x and y . Then when $t = t_{n+1} = (n + 1) dt$ the numerical scheme is given by:

$$T_M^{n+1} - T_M^n - \alpha_x dt (T_w^{n+1} - 2T_M^{n+1} + T_E^{n+1}) - \alpha_y dt (T_N^{n+1} - 2T_M^{n+1} + T_S^{n+1}) = dt F_M^{n+1} + T_M^n \tag{16}$$

$$\alpha_i \cdot x = \frac{\lambda_i dt}{C_i \rho_i \Delta x \Delta x} \quad \alpha_i \cdot y = \frac{\lambda_i dt}{C_i \rho_i \Delta y \Delta y} \tag{17}$$

where F_M^{n+1} is the heat source, C_i is the specific heat of the material i , ρ_i is the volume mass of the material i .

Table 2 Results of geometric dimensioning

Geometric parameters	Values
n	3
l_t	5.2 mm
t	50 μm
w	18.14 μm
d_{in}	162.12 μm
d_{out}	600 μm

Table 3 Results of electric dimensioning

Electrical parameters	Values
L_s	3.125 μH
R_s	0.12 Ω
C_s	0.0321 pF
$C_K1 = C_K2$	0.0648 pF
$R_{NiFe}1 = R_{NiFe}2$	5.32 k Ω
R_{Si}	0.49 m Ω
$C_{Si}1 = C_{Si}2$	0.276 pF

4 Results of Geometric, Electric and Thermal Dimensioning

All geometric, electric parameters that enter the dimensioning of the micro-coil are shown in the following summary Tables 2 and 3. This set of dimensions serves as our basis for the performance of the integrated micro coil. Results presented concern the geometric, electric and thermal dimensioning.

4.1 Influence of Geometric Parameters on the Behavior of Inductance

Figure 5 shows the influence of the frequency on the inductor for different widths w of the driver which vary from 10 to 100 μm . The inter-turn space s and the number of turns n are constant. We note that the decrease in the width of the conductor leads to an increase in the resistance of the conductor and therefore the increase of the current which has the effect of increasing the inductance.

Figure 6 shows the influence of the frequency on the inductance for different inter turns which vary from 60 to 120 μm . The value of the inductance is proportional to the square of the number of turns n while keeping the internal and external diameters constant. By increasing the number of turns, the length l_t increases or the inter-turn distance s decreases. In both cases the mutual inductance increases and consequently the inductance L .

Fig. 5 Inductance versus frequency

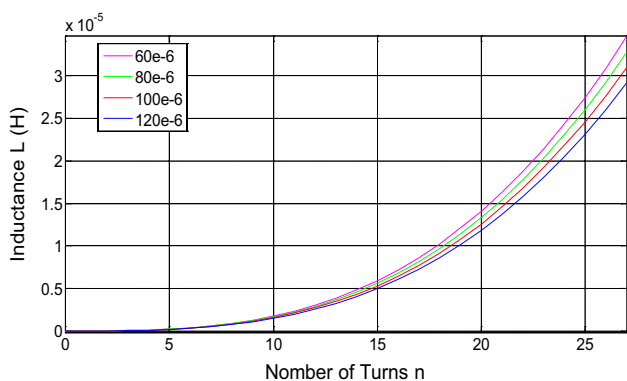
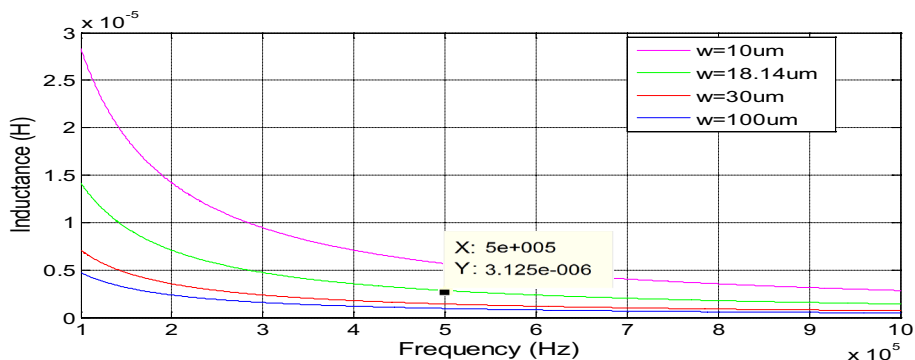


Fig. 6 Inductance versus number of turns

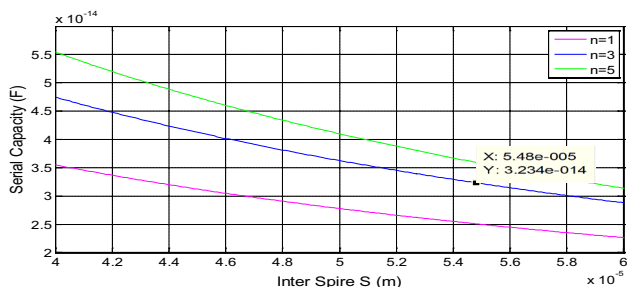


Fig. 7 Serial capacity versus Inter spires

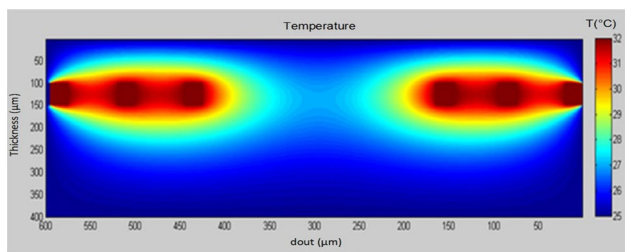


Fig. 8 Thermal mapping of the cross section of an integrated square spiral inductor

Figure 7 presents the variation of the series capacitance between the turns as a function of the inter-turn distance for different values of the number of turns. We note that the increase of the inter-turn space and the number of turns causes a decrease in the value of the series capacitance between the turns.

4.2 Results of Thermal Dimensioning

Figure 8 shows the distribution of the temperature of the component in the stationary state with the conditions contained in the specification (current flowing in the coil equal to $I_{max}=0.8$ A). Temperature is maximum and equal to 32 °C at the level of the conductors which are the source of heat. It decreases as one moves away to stabilize at 26 °C which corresponds to the ambient temperature.

4.3 Quality Factor

When the frequency increases several effects degrade the value of the quality factor of the inductor such as the skin effect, the losses in the substrate and the current flowing in the conductor [7]. All these effects depend on the geometry of the micro coil.

$$Q = \frac{\omega L_s}{R_s} \frac{R_p}{R_p + \left[\left(\frac{\omega L_s}{R_s} \right)^2 + 1 \right] R_s} \left[1 - \frac{R_s^2 (C_s + C_p)}{L_s} - \omega^2 L_s (C_s + C_p) \right] \tag{18}$$

$$R_p = \frac{1}{\omega^2 C_k^2 R_{Si}} + \frac{R_{Si} (C_k + C_{Si})^2}{C_k^2} \quad C_p = C_k \frac{1 + \omega^2 (C_k + C_{Si}) C_{Si} R_{Si}^2}{1 + \omega^2 (C_k + C_{Si})^2 R_{Si}^2} \tag{19}$$

After calculation, we have a quality factor Q equal to 78.23. From this below curve Fig. 9, can be deduced the value of inductance corresponding to the value of the quality factor corresponding to our working frequency.

Fig. 9 Quality factor versus frequency

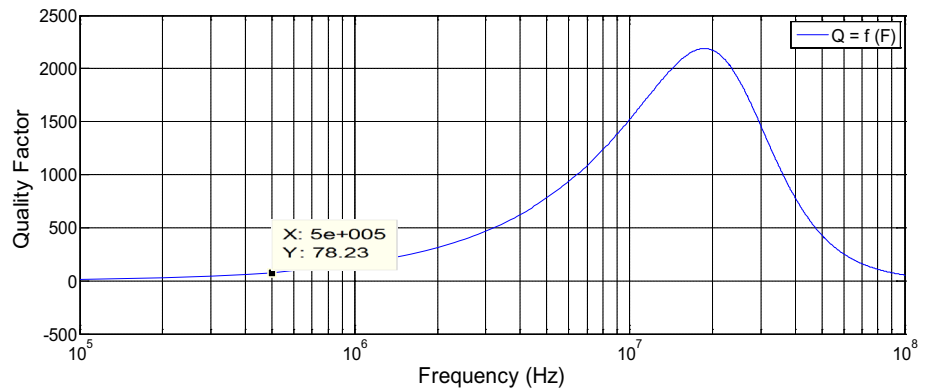
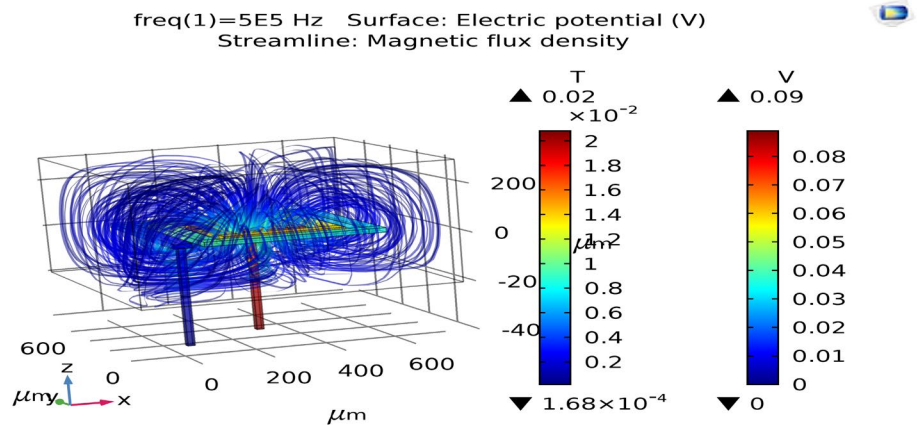


Fig. 10 Propagation of magnetic field lines in a planar micro-coil without magnetic core



4.4 3D Simulation of Magneto Dynamic Phenomena in Conductive Ribbons

4.4.1 Magnetic Flux Density Propagation Without Magnetic Core

Figure 10 shows the distribution of the density of the magnetic flux in the micro coil in the absence of the magnetic core. The absence of the magnetic core causes the field lines to be distributed in all directions, and are therefore not confined to the immediate vicinity of the micro-coil.

4.4.2 Magnetic Flux Density Propagation with Magnetic Core

Figure 11 shows the distribution of the density of the magnetic flux in our micro coil with a magnetic core. This latter confines the field lines, hence their optimal distribution in the immediate vicinity of the micro coil.

4.4.3 Current Density Distribution in the Micro-coil

Figure 12 shows the distribution of the current density in our coil. It is minimum at the exit of the coil because of the driver resistance value. On another hand, this density is

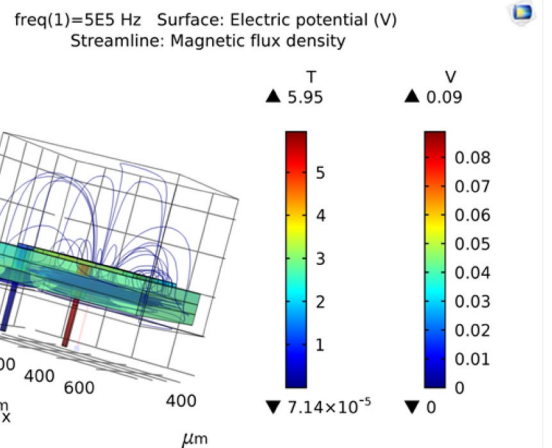


Fig. 11 Propagation of magnetic flux density in a planar micro-coil with a magnetic core

not uniform in this coil because it is more important at the angles that induce inhomogeneous resistances in the conductors [8]. It can also be observed that the effect of skin and proximity are present and manifest especially between adjacent turns.

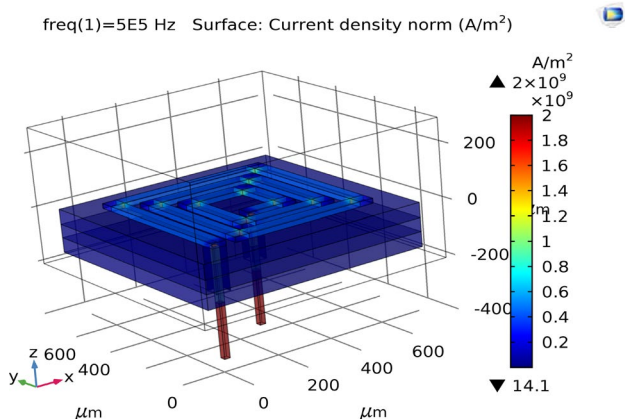


Fig. 12 Distribution of current density in the micro-coil

5 Micro-coil Manufacturing Process

The manufacturing process is presented for the implementation of an integrated inductance in a layer of magnetic material which comprises a substrate, a magnetic material and a coil of copper [5, 9, 10], the manufacturing process was made with the equipment available at Laplace laboratory (Fig. 13) outlines the steps of realization. Each step must be studied and optimized to ensure the performance and reproducibility of the process.

The manufactured coil is ultimately made of a copper conductor deposited on a magnetic layer of black color *NiFe* ferrite on a layer of silicon, all laid on the mass. In order to avoid any short circuit, a layer of white color Kapton insulation is placed between the two, Fig. 14. It has the following characteristics: surface of the magnetic circuit. 256 mm^2 , $w=0.85 \text{ mm}$, $t=35 \text{ }\mu\text{m}$, $d_{in}=12 \text{ mm}$, $d_{out}=16 \text{ mm}$, $s=2 \text{ mm}$, $n=3$.

6 Characterisation of the Realised Coil

Laboratory measure bench LAPLACE Fig. 15 is used, for the characterisation of the reels made. This bench consists of a LCR meter HP 419A, a software interface and acquisition, a current/voltage source [5]. The choice of the measurement model is made according to the impedance values predefined by the device and for each specified range. In the present case, the inductance values to be measured are of the order of a few μm . For this purpose, the equivalent circuit model shown in Fig. 15b has been chosen to take measurements.

Fig. 13 Manufacturing process of our micro coil

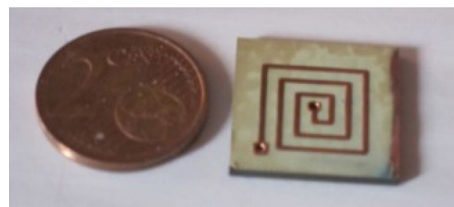
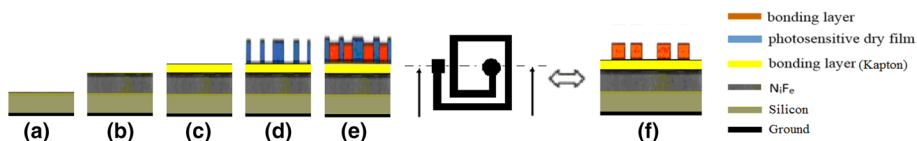


Fig. 14 realised inductor Inductance realized

7 Measurements Process

The different measurements made at the LAPLACE Laboratory [5, 10] on our micro-coil are on the module of Z , the angle of phase shift and the operating frequency for different values of gap which is the distance between the micro-coil and the top core Fig. 16c which allowed us to draw the following curves: L_s , R_s and C_s as a function of the frequency Fig. 16b. The frequency is from 100 Hz to 500 kHz. To the measurement of the gap, we used an insulating material (in black) of different thicknesses ranging from 0 to 1200 μm corresponding to the different gaps shown in Fig. 16c.

8 Results of measures

Figure 16 shows the evolution of the inductance as a function of the gap whose values vary from 0 to 1200 μm . Note the value of the inductance decreases as the gap increases. Beyond a certain value of the gap, the value of the inductance remains constant. It can be likened to a coil with virtually no hood. This leads us to conclude that to have a higher value of inductance, the best thing would be that it is to say contained in two cores. These results of measure were obtained for a frequency equal to 500 kHz.

8.1 Frequency Influence on the Inductance and Resistance for Different Gap Values

Figure 17 shows the evolution of the inductance as a function of frequency for different values of the gap. The frequency ranges from 100 Hz to 500 kHz. All these curves are grouped in the same graph, the inductance decreases as the gap increases. This is explained by the fact that when the nucleus on the upper face of the inductance moves away from it (increase the gap), there is a greater dispersion of

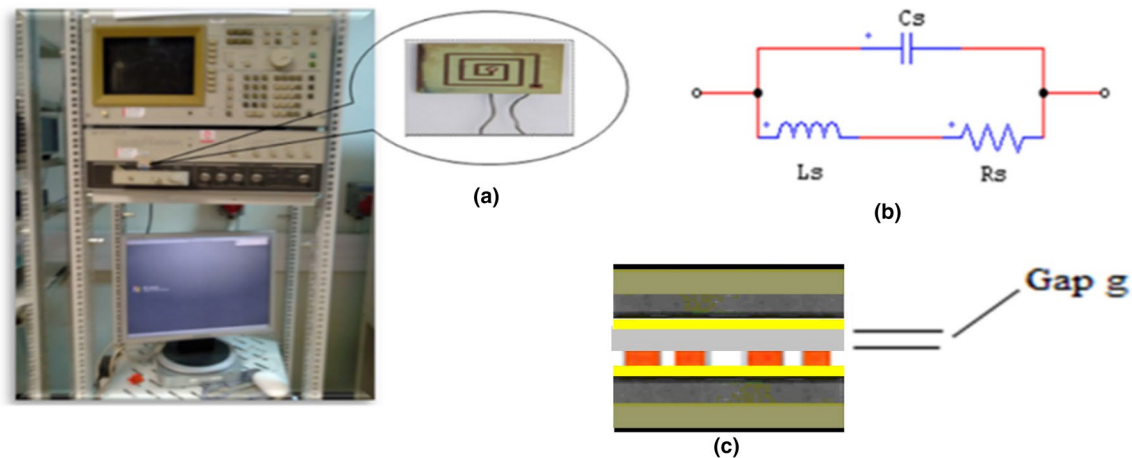


Fig. 15 Characterization bench (a), equivalent circuit model retained (b) and gap of the micro-coil (c)

Fig. 16 Variation of the inductance versus gap (results of measure)

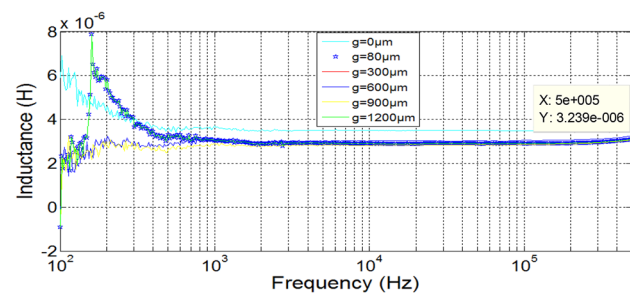
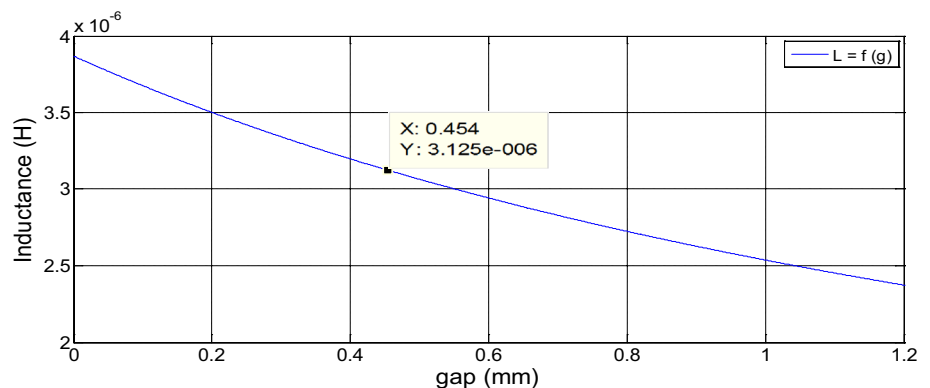


Fig. 17 Variation of the inductance as a function of frequency for different gap

the field lines, hence a decrease of the value of the inductance. Figure 18 shows the evolution of the series resistance of the coil with the frequency. The useful section of the wire decreases with frequency, under the skin's effect, therefore the resistance increases significantly with the frequency.

8.2 Frequency Influence on the Phase and the Module of the Impedance for Different Gap Values

Figures 19 and 20 respectively show the evolution of the phase shift and the modulus of the impedance as a function of frequency. Regarding the Fig. 19, regardless of the value of the gap, the same behavior is observed of the angle of phase shift, it rapidly increases the first frequency values to stabilize at a certain value, this whatever the value frequency. It shows the variation of the phase with the frequency. For large frequencies, it approaches 90° , this for all the thicknesses of the gap, which is correct. As the frequencies decrease, the phase should go up to 0° . As it is measurement results, the phase gets closer to 0° . From Fig. 20, the impedance modulus increases with frequency regardless the value of the gap.

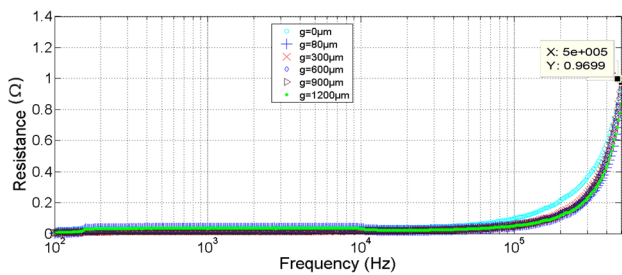


Fig. 18 Variation of the resistance as a function of frequency for different gap

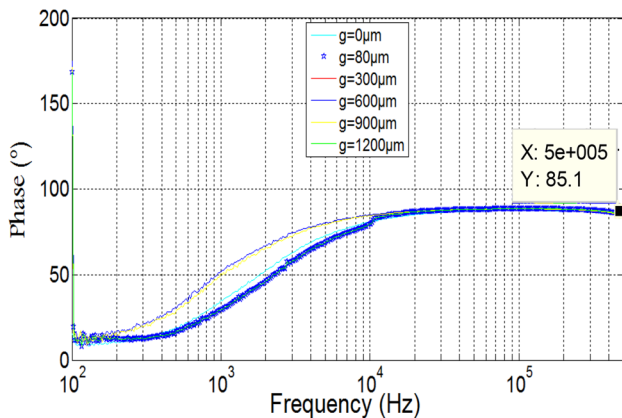


Fig. 19 The phase variation as a function of frequency for different gap

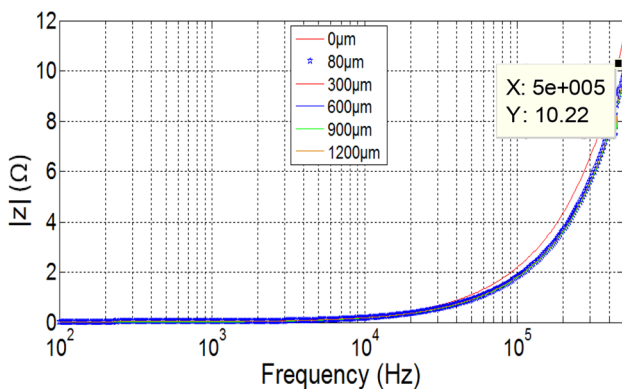


Fig. 20 Variation of the impedance module as a function of frequency for different gap

9 Result Validation

Figures 21a and 22a respectively show the evolution of induction and resistance of our coil as a function of

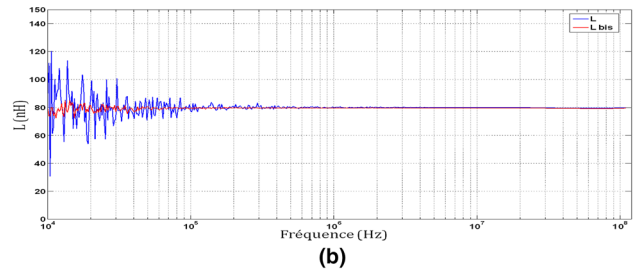
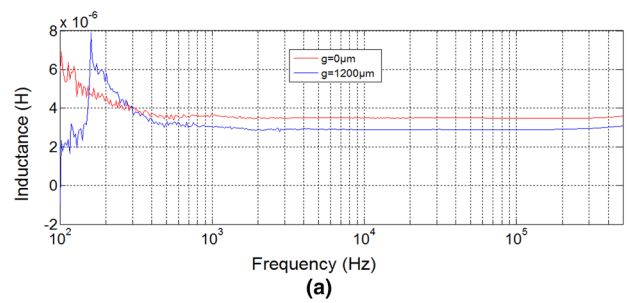


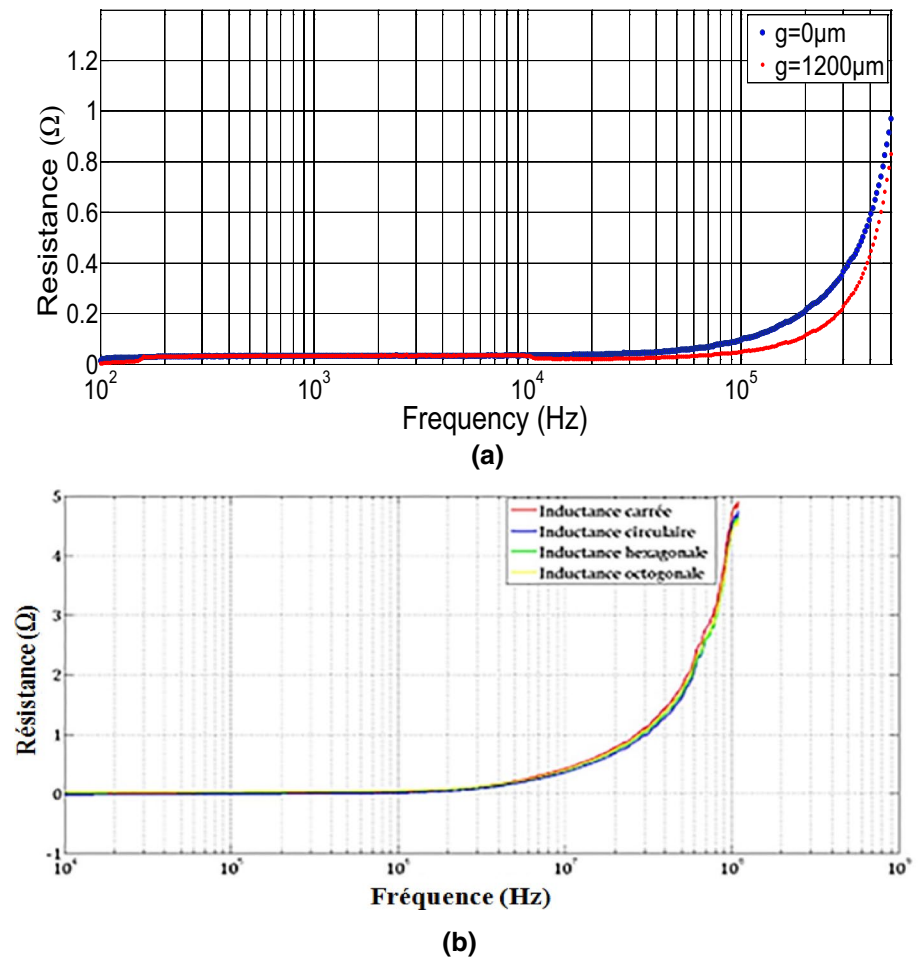
Fig. 21 Evolution of the inductance versus frequency, **a** our results, **b** issue of literature [5, 11]

frequency. To validate our dimensioning, we made a comparison of the results of our coil with a gap of 1200 microns with the coil (b) resulting from the literature we notice that the two gaits are identical. Indeed, in both figures, there are two areas corresponding to the transient and permanent regime. This comparison makes it possible to conclude that the sizing procedure and the implementation protocol are correct. This validates all the current work [5, 11].

10 Conclusion

The work presented in this paper focuses on the design, realization and characterization of a planar coil for square topology. The most important results found in the literature, relating to the techniques allowing the improvement of the characteristics of the planar coils are related either to the optimization of the topology of the inductance as well as its substrate. As an indication, the proximity effects increase with the width of the turns. The starting point of the dimensioning of this coil is the specifications of a micro converter in which we will integrate this coil. The results of magneto dynamic and thermal simulation, having validated the geometrical and electrical dimensioning, we went to the stage of realization of this coil with a magnetic circuit (spiral on the Kapton which plays the role of insulator, and on the ferrite which plays the role of magnetic circuit). The various stages of implementation of this coil as well as its characterization were conducted at the laboratory Laplace–Toulouse. Measurements focused on impedance and phase versus frequency. This allowed to determine the series resistance and series

Fig. 22 Evolution of the resistance versus frequency, **a** our results, **b** issue of literature [5, 11]



inductance of this coil. The measurements allowed to follow the evolution of the impedance Z , the inductance L_s and the resistance R_s as a function of frequency for different gap values. In order to validate the results found in this paper a comparison with those from the literature is done and shows similarities between the two works.

References

1. H.A. Wheeler, Simple inductance formulas for radio coils. Proc. IRE **16**(10), 1398–1400 (1928)
2. S. Mohan et al., Simple accurate expressions for planar spiral inductances. IEEE J. Solid State Circuits **34**(10), 1419–1424 (1999)
3. P. Spiteri [AF 501] *Méthode des différences finies pour les EDP d'évolution*, Techniques de l'ingénieur (2002)
4. A. Allaoui, A. Hamid, P. Spiteri, V. Bley, T. Lebey, Thermal Modeling of an Integrated Inductor in a Micro-Converter. J. Low Power Electron. **11**(1), 63–73 (2015)
5. Laboratory on Plasma and Conversion of Energy-UMR5213, Toulouse, France
6. R. Melati, A. Hamid, T. Lebey, M. Derkaoui, Design of a new electrical model of a ferromagnetic planar Inductor for its integration in a micro converter. Math. Comput. Model. **57**(1–2), 200–227 (2013)
7. C.P. Yue, *On-chip spiral inductors for silicon-based radio-frequency integrated circuits*, PhD thesis partial fulfilment, Stanford University, 1998
8. K. Murata, T. Hosaka, Y. Sugimoto, in *Effect of a ground shield of a silicon on-chip spiral inductor*, Asia-Pacific Microwave Conference, 2002, p. 177–180
9. X.-N. Wang, X.-L. Zhao, Y. Zhou, X.-H. Dai, B.-C. Cai, Fabrication and performance of novel RF spiral inductors on silicon. MicroElectron. J. **36**, 737–740 (2005)
10. E. Haddad, M. Christian, B. Allard, M. Soueidan, C. Joubert, in *Micro-fabrication of planar inductors for high frequency DC-DC power converters*, ed. by L. Malkinski, Advanced magnetic materials, 2012, p. 119–132
11. E. Haddad, *Conception, Réalisation et Caractérisation d'Inductances Intégrées haute fréquence*, Thèse soutenue en 2012
12. B. Estibals, A. Salles, Design and realisation of integrated inductor with low DC-resistance value for integrated power applications. HAIT J. Sci. Eng. B **2**(5–6), 848–868 (2005)
13. A.S. Royet, R. Cuchet, D. Pellissier, P. Ancey, On the investigation of spiral inductors processed on Si substrates with thick porous Si layers. ESSDERC **D5**(111), 2003 (2003)
14. Deleage O., *Conception, réalisation et mise en œuvre d'un micro-convertisseur intégré pour la conversion DC/DC*, Thesis (Grenoble, France, 2009)

15. S. Couderc, *Etude de matériaux ferromagnétiques doux à forte aimantation et à résistivité élevée pour les radiofréquences. Applications aux inductances spirales planaires sur silicium pour réduire la surface occupée*, Thèse Soutenue (2006)

Publisher's Note Springer Nature remains neutral with regard to jurisdictional claims in published maps and institutional affiliations.